Plankton community responses to pulsed upwelling events in the southern Taiwan Strait

Yanping Zhong[1,2,3], Jun Hu[1,2,3,4], Edward A. Laws[5], Xin Liu (iD) [1,2,3]*, Jixin Chen[1,2,3], and Bangqin Huang[1,2,3]

[1]Fujian Provincial Key Laboratory of Coastal Ecology and Environmental Studies, Xiamen University, Xiamen 361102, China
[2]Key Laboratory of Ministry of Education for Coastal and Wetland Ecosystems, Xiamen University, Xiamen 361102, China
[3]College of the Environment and Ecology, Xiamen University, Xiamen 361102, China
[4]Shanghai Qingpu Environmental Monitoring Station, Shanghai 201700, China
[5]Department of Environmental Sciences, School of the Coast & Environment, Louisiana State University, Baton Rouge, LA 70803, USA

*Corresponding author: tel: + 86 592 218 1151; e-mail: liuxin1983@xmu.edu.cn.

We used field observations (mapping and time-series observations) and satellite data to investigate the changes of environmental factors and plankton community structure during four pulsed upwelling events in the southern Taiwan Strait (STWS) during August 2004 and July 2005. Based on the surface temperature, salinity, and concentrations of nitrate, oxygen, and chlorophyll a (Chl a), we identified three stages of upwelling: recent, mature, and aged upwelled water. Diatoms and Synechococcus dominated during the first two and third stages of the upwelling, respectively. In recently upwelled water, phytoplankton grew rapidly, and nutrient concentrations were relatively high. Diatoms accounted for >69% of the total Chl a in recently upwelled and mature water. As the upwelled water aged, the phytoplankton community shifted to coexistence of diatoms and Synechococcus. The microzooplankton community was dominated by aloricate ciliates and tintinnids during upwelling, but the abundance of heterotrophic dinoflagellates increased as the upwelled water matured. Microzooplankton grazing reached a maximum during the mature stage and approximately balanced phytoplankton growth in aged, upwelled water. Overall, our study revealed rapid changes in the plankton community during the different stages of upwelling that reflected the complex and dynamic nature of upwelling systems.

Keywords: coastal upwelling, diatoms, microzooplankton, phytoplankton community, southern Taiwan Strait, Synechococcus.

Introduction

Marine phytoplankton account for nearly half of primary productivity in the biosphere (Field et al., 1998), and changes of phytoplankton abundance and composition are closely related to the various biotic and abiotic factors that characterize aquatic ecosystems (Widdicombe et al., 2010). Upwelling ecosystems, which are the most productive regions of the ocean, are characterized by inputs of nutrient-rich subsurface water into the euphotic zone that stimulate phytoplankton production and induce a shift of the biological community (Mitchell-Innes and Walker, 1991). In upwelling systems, changes in environmental conditions such as temperature, nutrient availability, turbulence, and irradiance may occur abruptly and lead to a rapid succession of phytoplankton species and alteration of phytoplankton community composition. Numerous studies have documented changes of phytoplankton communities on seasonal or interannual timescales in upwelling ecosystems (Oh et al., 2004; Silva et al., 2009; Lips and Lips, 2010; Du and Peterson, 2013). For instance, Du and Peterson (2013) described how the upwelling that occurs from approximately March to October in the northern California Current causes changes in phytoplankton biomass and composition following the upwelling/downwelling cycles. Diatoms can contribute as

much as 80% of phytoplankton biomass during upwelling, but dinoflagellates dominate the phytoplankton community at the end of upwelling. Silva *et al.* (2009) have also suggested that the phytoplankton communities in Lisbon Bay (Portugal) change with the seasonal variations of upwelling.

Short-term responses associated with pulsed upwelling events have not received comparable attention, and current understanding of such responses is based primarily on studies in eastern boundary current upwelling systems (EBCUS), where the durations of one upwelling event can be a few days to a few weeks (Brown and Hutchings, 1987; Mitchell-Innes and Walker, 1991; Hansen *et al.*, 2014). Three stages characterized by nutrient concentrations and phytoplankton biomass are typically observed during an integral upwelling event: recently upwelled water, mature upwelled water, and aged upwelled water (Brown and Hutchings, 1987). In the southern Benguela upwelling system, Mitchell-Innes and Walker (1991) identified two upwelling cycles during a 27-day period at a fixed station. The phytoplankton composition varied with environmental changes during the different stages, from small diatoms to large diatoms then to dinoflagellates (Mitchell-Innes and Walker, 1991; Walker and Peterson, 1991). Temperature, salinity, the oxygen concentration of the surface water, and the extent of nutrient consumption have been used to characterize the upwelling stages (Takahashi *et al.*, 1986; Hansen *et al.*, 2014; Mohrholz *et al.*, 2014).

Several theories have been put forward to explain that phytoplankton succession results from changes along environmental gradients. Margalef's classical mandala (1978) attributes the dominance of different phytoplankton groups to different nutrient-turbulence spaces. His theory is consistent with phytoplankton succession from diatoms to dinoflagellates during upwelling events (Chapman and Bailey, 1991; Mitchell-Innes and Walker, 1991). Reynolds (1984) applied Grime's CSR theory (Competitor, Stress tolerator, and Ruderal; Grime, 1977) to fresh-water phytoplankton and identified different functional phytoplankton groups based on the strategies that explain their responses to environmental conditions. More recently, trait-based phytoplankton community ecology has been used to explain community and/or species responses to environmental changes based on functional traits (Litchman *et al.*, 2012). Common among all the above-mentioned theories is a focus on abiotic variables, but regulation of phytoplankton succession during an upwelling event also reflects top-down control from microzooplankton, zooplankton, or small fish (Tilstone *et al.*, 2000). The traditional view is that upwelling systems are characterized by short food chains in which large phytoplankton are consumed directly by mesozooplankton or small fish. However, grazing by microzooplankton is also an effective form of top-down control that impacts phytoplankton biomass and composition in upwelling areas (Teixeira *et al.*, 2011). In fact, some studies have suggested that microzooplankton herbivory can remove most of primary production in upwelling systems (Neuer and Cowles, 1994; Fileman and Burkill, 2001; Huang *et al.*, 2011). Nevertheless, few studies have concerned the temporal variability of the microzooplankton community and its impact on the dynamics of phytoplankton communities during the different phases of upwelling.

The Taiwan Strait, which is bounded by southeastern mainland China and Taiwan Island, is an important channel between the East China Sea (ECS) and the South China Sea (SCS; Figure 1a). Its complex hydrology reflects the influence of the East Asian monsoons and their seasonal variability

(Hong *et al.*, 2011). The southwesterly winds that blow over the southern Taiwan Strait (STWS) and its complex topography produce many upwelling regions, including the Dongshan upwelling (Figure 1a), Taiwan Bank upwelling, and Penghu upwelling (Hong *et al.*, 2011). The mechanisms that drive upwelling differ in the STWS and EBCUS. Upwelling in the latter occurs throughout most of the year and is caused by a combination of Ekman transport induced by the equatorward Trade Windstress and the Coriolis force (Fréon *et al.*, 2009). In contrast, coastal upwelling in the STWS occurs from June to August and is influenced by southwesterly winds and topographic effects (Hong *et al.*, 2011). Currents in the STWS are quite complex, and at least three different types of upwelled water masses are found there (Tang *et al.*, 2004). Furthermore, some studies have shown that the upwelled water near Dongshan is transported from Shanwei (Figure 1a), where the upwelled water comes from depths of 50–100 m in the SCS (Gan *et al.*, 2009a), and the nutrient concentrations are lower in that upwelled water than in the EBCUS (Hu *et al.*, 2015). More importantly, upwelling in the STWS, which can change markedly in a short time and often persists for 7–12 days (Shang *et al.*, 2004), is related to wind patterns (Zhang *et al.*, 2011).

We have previously observed the spatio-temporal variations of coastal upwelling events and associated phytoplankton biomass responses in the STWS by using a combination of satellite and field data (Hong *et al.*, 2009, 2011; Jing *et al.*, 2009). However, because of the limitations of *in situ* time-series observations, little is known about the rapid succession of phytoplankton and zooplankton communities in response to changes of environmental conditions during a pulsed upwelling event in costal upwelling systems where the mechanisms responsible for the upwelling and the nutrient concentrations differ from those in EBCUS. In this study, we therefore focused on the differences between the plankton communities during the three upwelling stages and were able to explain the mechanisms likely responsible for the succession of phytoplankton communities based on a combination of bottom-up and top-down controls.

Material and methods
Study areas and sites
The study areas were in the STWS (Figure 1). The RV Yanping 2 was used to collect samples during two summer cruises from 29 July to 7 August 2004 (Figure 1b) and during 5–14 July 2005 (Figure 1c). To better understand how the phytoplankton community responded to the different stages of upwelling, daily time-series observations were conducted at stations (Stns.) F1 (23°50′59.3″; 118°06′03.5″, 35 m in depth) and F3 (23°44′31.2″; 118°13′22.9″, 48 m in depth) during 1–5 August 2004 as well as at station B1 (20°12′24.36″; 117°18′13.7″, 49 m in depth) on 5, 6, 8, 9, 10, and 12 July 2005.

Measurements of hydrological and chemical parameters
Temperature (T) and salinity (S) were recorded *in situ* with a CTD system (Seabird SEB 19). Dissolved oxygen (DO) in seawater was determined by the method described in Strickland and Parsons (1972). All nutrient and biological samples were collected in at least three layers within the euphotic zone. Samples for nutrient analysis were collected in 100-ml polypropylene bottles, with 15, 17, and 23 samples at Stns. F1, F3, and B1 during the observations, respectively. The nutrient concentrations were measured with a flow injection analyzer (Tri-223 AutoAnalyzer;
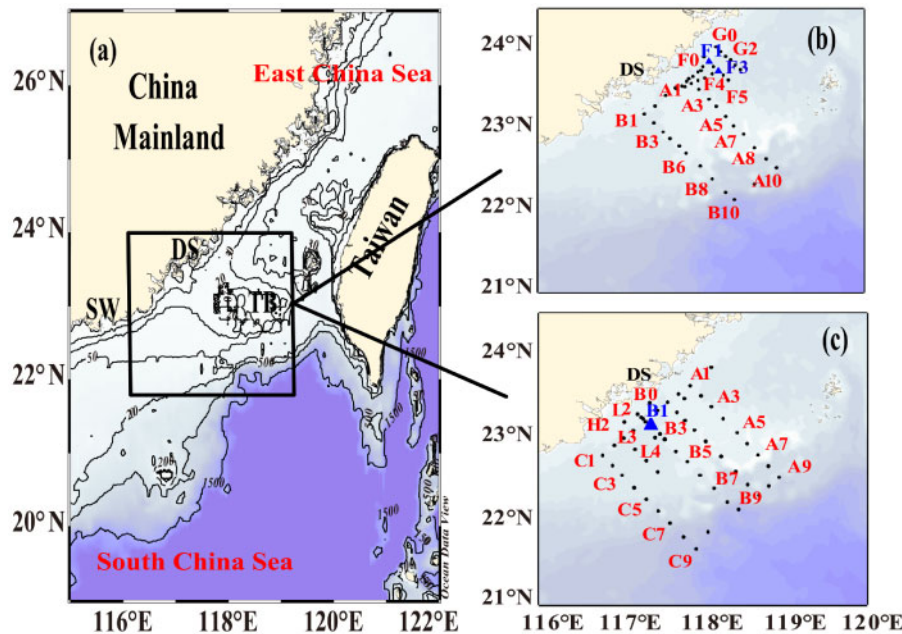
Figure 1. Study areas (a) and sampling stations (b, c) in the southern Taiwan Strait during summer cruises of 2004 and 2005. (a) Study areas are the solid lined rectangular areas; DS, Dongshan; SW, Shanwei; TB, Taiwan Bank. (b) Sampling stations during the 2004 summer cruise. (c) Sampling stations during the 2005 summer cruise. All stations measured hydrological parameters, and stations marked with names are comprehensive stations, which measured hydrological, nutrients, and biological parameters. Stns. F1 and F3 were time-series tracking stations in 2004, whereas Stn. B1 was time-series tracking station in 2005.

Pai *et al.*, 1990a, b). The detection limits for nitrate, nitrite, phosphate, and silicate were 0.2, 0.08, 0.17, and 0.19 μmol l^{-1}, respectively. Nutrient concentrations below the detection limits were recorded as the detection limits.

Measurements of Chl *a* and phytoplankton composition

Aliquots of 200–500 ml of seawater were first filtered through 25-mm GF/F filters (Whatman) for Chl *a* analysis, and the filters stored in liquid nitrogen. In the laboratory, they were stored in a freezer at −80°C until analysis. The Chl *a* concentrations were determined by florescence analysis after the pigments were extracted in 90% acetone for 24 h at −20°C (Parsons, 1984). Aliquots of 1–4 l of seawater were filtered through 25-mm GF/F filters for the analysis of photosynthetic pigments (<50 mm Hg) and stored in the same way as the Chl *a* samples. Each filter was freeze-dried and extracted with 1 ml of *N*, *N*-dimethylformamide at −20°C. The extract was then mixed with ammonium acetate in equal proportions. Pigment concentrations were measured by high-performance liquid chromatography (HPLC). Finally, the CHEMTAX calculations and procedures reported by Mackey *et al.* (1996) were used to determine the relative contributions of nine different phytoplankton groups to the total Chl *a* (Mackey *et al.*, 1996; Pinckney *et al.*, 1998). The nine phytoplankton groups were dinoflagellates (Dino), diatoms (Diat), haptophytes (Type 8; Hapt.T8.), haptophytes (Type 6; Hapt.T6.), chlorophytes (Chlo), cryptophytes (Cryp), *Prochlorococcus* (Proc), *Synechococcus* (Syne), and *prasinophytes* (Pras).

Phytoplankton samples for microscopic analysis were also collected. Water samples (1 l) were fixed with Lugol's iodine, allowed to settle for 24 h, then further concentrated to 10 ml (Utermöhl, 1958). After thorough mixing, a 0.1-ml subsample was placed in a 0.1-ml (20 ×20 mm) counting chamber and observed under an

optical microscope (×400 magnification, Leica, MRC1024) to identify the dominant species (Tomas, 1997).

Microzooplankton abundance and dilution dataset

Information on microzooplankton abundance, phytoplankton growth rates, and microzooplankton grazing rates were extracted from published datasets (Zeng *et al.*, 2006; Tian, 2007; Xiang, 2009; Huang *et al.*, 2011; Zeng and Huang, 2012) that are presented in Supplementary Tables S1 and S2. Phytoplankton growth rates (k) and microzooplankton grazing rates (g) in surface waters were estimated by the dilution method (Landry *et al.*, 1995). The pressure of microzooplankton grazing on phytoplankton was represented by the ratio of g:k. Microzooplankton was classified into four groups: aloricate ciliates, tintinnids, heterotrophic dinoflagellates, and copepod nauplii.

Monthly windspeed, sea surface temperature, and Chl *a* derived from satellite

Monthly average windspeeds (Wind, m s^{-1}) during the cruises were extracted from the Cross-calibrated Multi-Platform database (available at http://data.remss.com/ccmp/). Monthly average sea surface temperature (SST) and Chl *a* in the TWS during August 2004 and July 2005 were derived from the Moderate Resolution Imaging Spectroradiometer (MODIS) database (available at https://oceancolor.gsfc.nasa.gov/).

Statistical analyses

All statistical analyses were done using R software version 3.4.3 (Core, 2014). The "Vegan" and "Cluster" packages in R were used to carry out the redundancy analysis (RDA) and cluster analysis. The cluster analysis was used to distinguish different

stages of upwelling, and the optimal numbers of clusters can be obtained from the K value via the function NbClust based on the distance between samples. Generalized additive models (GAMs) fitted with the "mgcv" package are the extension of generalized linear models, which do not require that parameter values be set in advance and are smooth functions of explanatory variables (Wood, 2004). In our study, we established only a univariate GAM based on the formation $Y = \alpha + s(X) + \varepsilon$. In this formation, Y represents one of the response variables, including the absolute concentrations of diatoms and *Synechococcus*. The function $s(X)$ is a non-linear function based on cubic regression splines, and X represents one of the predictors [temperature, silicate, nitrate+nitrite (NO_x), and the ratio of silicate to NO_x]. The parameters α and ε represent the intercept and error, respectively. The RDA and GAMs analyses were conducted based on the combined dataset from the two cruises. Figures 1, 3, 4, and 5 were plotted with Ocean Data View software (Schlitzer, 2015).

Results

Horizontal distributions of hydrological parameters

Figure 2 shows the monthly average SST and surface Chl *a* from MODIS in the TWS during August 2004 and July 2005. The distribution patterns in both years were similar and revealed low temperatures and high Chl *a* concentrations indicative of upwelled waters in the coastal zones and the Taiwan Bank (Figure 2). However, significant differences in the upwelling regions were apparent between August 2004 and July 2005. The larger areas of low temperatures and high Chl *a* concentrations in July 2005 vs. August 2004 indicated that upwelling was overall stronger in July 2005 than in August 2004.

The distributions of temperature in the surface water during summer cruises of 2004 and 2005 were similar to those derived from satellite data (Figure 3). SST (Figure 3a and d) varied from 24.6 to 29.3°C in August 2004 and from 22.3 to 30.5°C in July 2005. The relatively cold ($T < 27$°C), saline ($S > 33.8$) water with high Chl *a* concentrations (up to $1.5\,\mu g\,l^{-1}$) was found near Dongshan Island and at Stns. F1 and F3 in 2004 (Figure 3a–c) and indicated that the two sites were affected by upwelling. In July 2005, the surface water near Dongshan, including Stn. B1, was also relatively cold ($T < 25$°C), saline upwelled water, and the Chl *a* concentrations were high (Chl $a > 2.0\,\mu g\,l^{-1}$). During July 2005, however, the surface in the nearshore area of the C section was relatively warm ($T > 28$°C), low-salinity ($S < 31$) water from the Pearl River plume.

Figure 4 shows the T–S diagrams during the two summer cruises of 2004 and 2005. During the 2004 cruise, the study areas were influenced mainly by SCS water, and subsurface and near-surface SCS water appeared at Stns. F1 and F3, respectively. The implication is that Stn. F1 was strongly influenced by upwelling, whereas Stn. F3 was less influenced. Conditions at many stations were similar in 2004 and 2005, and the fact that the characteristics of the surface water at Stn. B1 were the same as those of the SCS subsurface water indicated that Stn. B1 was also influenced by upwelling. A few stations were concurrently characterized by low-salinity, warm water from the Pearl River plume ($S < 31$, Figures 3e and 4b).

Evolution of upwelling and associated hydrological conditions and concentrations of nutrients and Chl *a*

The water at Stns. B1 and F1 was similar to the SCS subsurface water, whereas water at Stn. F3 resembled the SCS near-surface water (Figure 4). The implication is that upwelling was stronger at Stns. B1 and F1 than at Stn. F3. This conclusion is consistent with the hydrological parameters and phytoplankton biomass (Figure 5). During 5–10 July 2005, the surface water at Stn. B1 was influenced by the Pearl River plume and was therefore warm ($T > 26$°C) with a low-salinity ($S < 31$). In contrast, the water below 10 m was upwelled water with a low temperature ($T < 23$°C) and high salinity ($S > 34$). During 10–12 July the upwelling was more pronounced, and upwelled water reached the surface (Figure 5a and b). The development of an upwelling event was therefore observed during the July 2005 surveys at Stn. B1. From 1 to 5 August 2004, we observed a clear increase in temperature from ~24 to 27°C and decline in salinity from 34.05 to 33.80 at Stn. F1. A slight increase in temperature from ~25 to 28°C also occurred at Stn. F3, but without an obvious change in salinity. Upwelling intensities at Stns. F1 and F3 during 1–5 August 2004 were therefore relatively low.

Spatio-temporal changes in nutrient concentrations throughout the water column at Stns. B1, F1, and F3 were very dynamic (Figure 6). The median of nitrate and silicate concentrations in the water column on 12 July 2005 were higher at Stn. B1 than at Stns. F1 and F3, whereas phosphate concentrations were always below the limit of detection in the water column at Stn. B1. Nitrate and silicate concentrations in the water column at Stns. F1 and F3 were extremely low; they varied from below the detection limit to $0.73\,\mu mol\,l^{-1}$ and 0.50–$4.06\,\mu mol\,l^{-1}$, respectively. The phosphate concentrations in the water column at Stns. F1 and F3 decreased over time, and finally were below the detection limit.

Figure 5 shows the temporal variations of Chl *a* concentrations throughout the water column at three stations based on HPLC analysis. The Chl *a* concentrations at Stn. B1 were relatively constant between 5 and 10 July but increased rapidly after 10 July. The highest Chl *a* concentration ($5.45\,\mu g\,l^{-1}$) was observed at a depth of 10 m on 12 July. At Stn. F1, the Chl *a* concentrations increased from 1 to 2 August 2004, reached a maximum of $2.36\,\mu g\,l^{-1}$ at a depth of 30 m, then decreased between 3 and 5 August. The Chl *a* concentrations at Stn. F3 decreased from $1.80\,\mu g\,l^{-1}$ at 10 m depth on 1 August to $0.29\,\mu g\,l^{-1}$ at 40 m on 5 August.

Dynamics of phytoplankton and microzooplankton community during the different stages of upwelling

We identified four clusters and three stages of upwelling via cluster analysis (Figure 7 and Table 1) based on the surface temperature, salinity, and concentrations of oxygen, nutrients, and Chl *a* (Stns. F1 and F3 in 2004, Stn. B1 in 2005, and adjacent station Stn. A1 in 2004 and 2005). Between 5 and 10 July 2005, Stn. B1 was influenced by the Pearl River plume, with low mean surface salinity ($S < 31$), and relatively high Chl *a* concentration ($1.56\,\mu g\,l^{-1}$). The conditions at Stns. A1 on 14 July and B1 on 12 July 2005, when the mean surface temperature (23.63°C), oxygen concentration ($6.97\,mg\,l^{-1}$), and Chl *a* concentration ($1.17\,\mu g\,l^{-1}$) were relatively low, could be described as the first phase of an upwelling event (recently upwelled water). The conditions at Stn. A1 on 29 July and F1 on 1 August 2004, when the mean surface temperature (25.04°C), oxygen concentration ($8.15\,mg\,l^{-1}$), and Chl *a* concentration ($1.39\,\mu g\,l^{-1}$) were increasing, could be considered the second phase (mature upwelled water). The conditions at Stns. F1 and F3 during 2–5 August 2004, when the
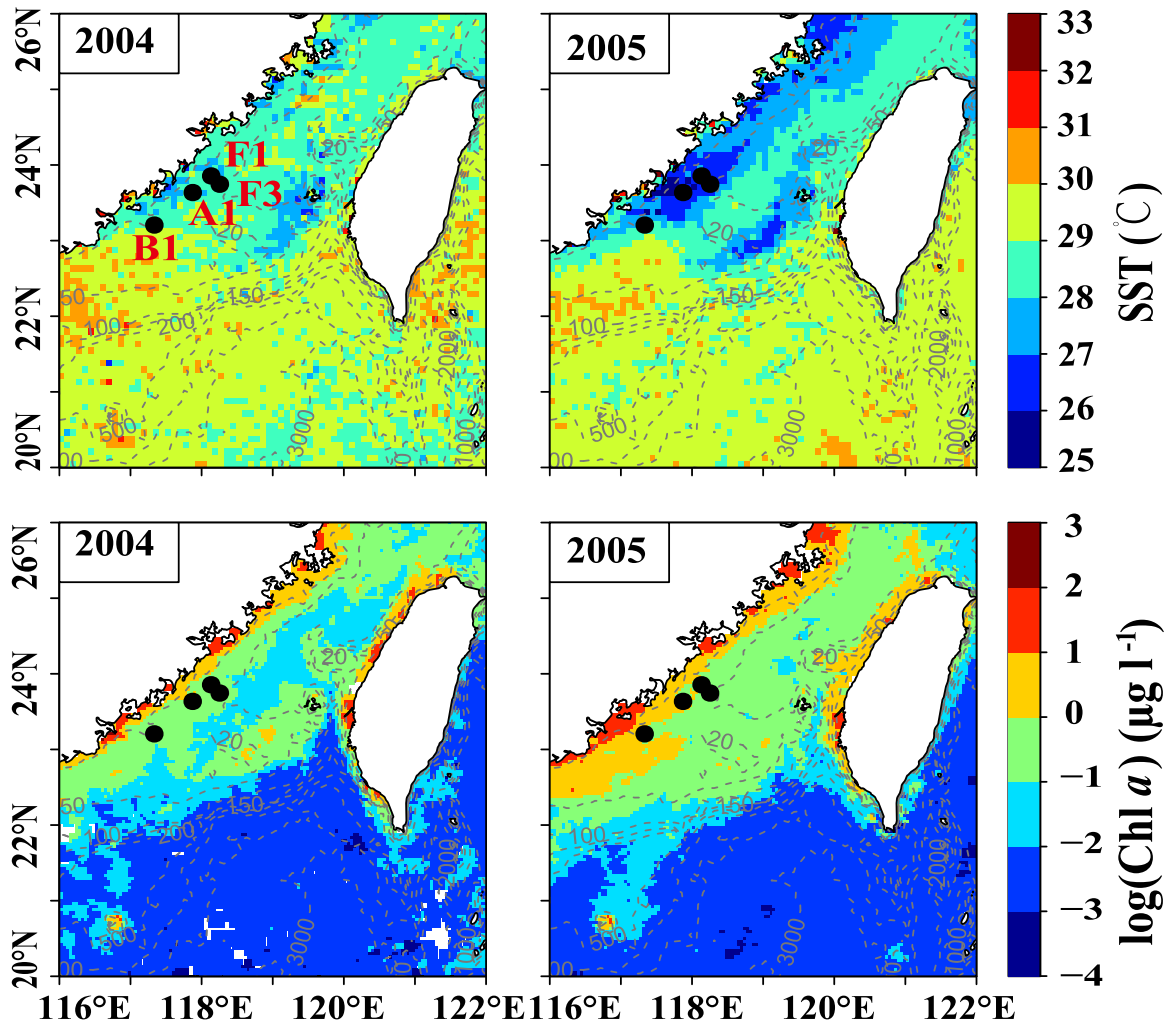
Figure 2. Monthly average sea surface temperature (SST, upper panels) and surface Chl *a* (lower panels) from MODIS database in the Taiwan Strait during August 2004 and July 2005. Stations marked with names were time-series tracking stations (Stns. F1, F3, and B1) and their nearby Stn. A1 during summer cruises of 2004 and 2005.

temperature ($26.82°C$) and oxygen concentration ($8.80\,\mathrm{mg\,l^{-1}}$) were high, and the Chl *a* ($0.80\,\mathrm{\mu g\,l^{-1}}$) and nitrate concentrations ($0.13\,\mathrm{\mu mol\,l^{-1}}$) were decreasing, corresponded to the third phase (aged upwelled water).

We calculated the average depth-integrated phytoplankton biomass and composition to better understand phytoplankton changes during the different stages of upwelling (Figure 8). Diatoms were the dominant phytoplankton group in the first stage. They accounted for 76% of the total Chl *a*. Microscopic analysis revealed that the diatoms at Stn. B1 on 12 July 2005 consisted of species such as *Pseudo-nitzschia delicatissima*, *Pseudo-nitzschia pungens*, *Rhizosolenia fragilissima*, *Asterionella japonica*, *Skeletonema costatum*, *Thalassionema nitzschioides*, and *Leptocylindrus danicus*. During the second stage, the average depth-integrated Chl *a* concentrations increased. Diatoms were still major contributors and accounted for 69% of the total Chl *a*, but the proportion of *Synechococcus* increased slightly, from 4 to 11%. During the third phase, the contribution of diatoms decreased further to 41%, and the proportion of *Synechococcus* increased significantly to as much as 31%. The main diatom species were *Asterionellopsis glacialis*, *S. costatum*, *T. nitzschioides*,

P. delicatissima, and *Chaetoceros* spp. Analysis of the microzooplankton datasets (Supplementary Tables S1 and S2) revealed that the average depth-integrated microzooplankton biomass increased slightly, from 1338 to 1884 ind.l^{-1}, as the upwelling relaxed. The major microzooplankton during upwelling was aloricate ciliates and tintinnids, which accounted for at least 79% of microzooplankton abundance (Figure 9a). The proportion of aloricate ciliates reached a maximum of 68% of microzooplankton abundance during the second stage. As the upwelled water aged, the contribution of heterotrophic flagellates increased from 4 to 14% of microzooplankton abundance.

Figure 9b shows the calculated mean phytoplankton growth rates and microzooplankton grazing rates during the different upwelling phases. The phytoplankton growth rates in the first two stages were high, up to $1.06\,\mathrm{d^{-1}}$. Microzooplankton grazing in the first stage ($0.65\,\mathrm{d^{-1}}$) and its pressure on phytoplankton ($g{:}k = 0.58$) were low. During the second stage, microzooplankton grazing reached a high level and put strong pressure on phytoplankton ($g{:}k = 1.2$). In the third phase, phytoplankton growth rates ($0.67\,\mathrm{d^{-1}}$) and microzooplankton grazing rates ($0.64\,\mathrm{d^{-1}}$) were lower and approximately equal.
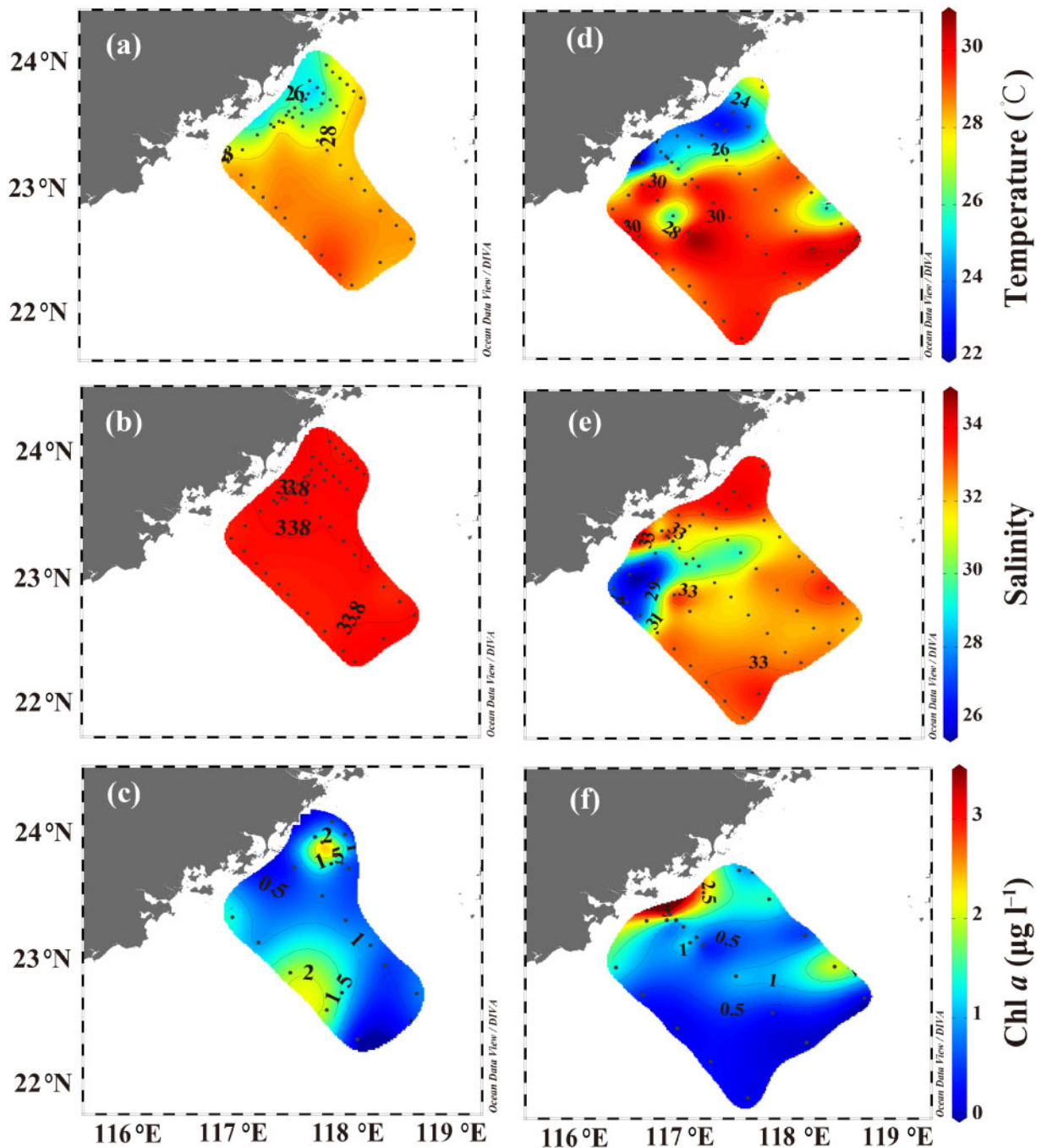
Figure 3. Horizontal distribution of surface temperature (°C, a, d), salinity (b, e), and Chl *a* concentrations (µg l⁻¹, c, f) during summer cruises of 2004 (left panels) and 2005 (right panels) in the southern Taiwan Strait. Stations marked with names were time-series tracking stations (Stns. F1, F3, and B1) and their nearby Stn. A1 during summer cruises of 2004 and 2005. DS, Dongshan.

Statistical and model analysis

RDA analysis was used to discern the relationships between the phytoplankton community and environmental metrics (Figure 10a). The environmental metrics explained 36.4% of the variance of the phytoplankton communities in the up-welling systems. The first two axes accounted for 29.0 and 7.4% of the variance, respectively. Diatoms, which were located on the negative side of the first RDA axis, were positively correlated with monthly windspeeds and nutrient concentrations. Conversely, *Synechococcus*, which was located on the positive side of the first RDA axis, was better explained by temperature and was relatively unaffected by silicate, nitrate+nitrite (NO$_x$), and phosphate. Dinoflagellates as well as other phytoplankton groups, such as prasino-phytes, cryptophytes, haptophytes (type 6), and chlorophytes, were located in the middle of the RDA plot (Figure 10a), the implication being that their relative abundances were insensi-tive to environment changes.
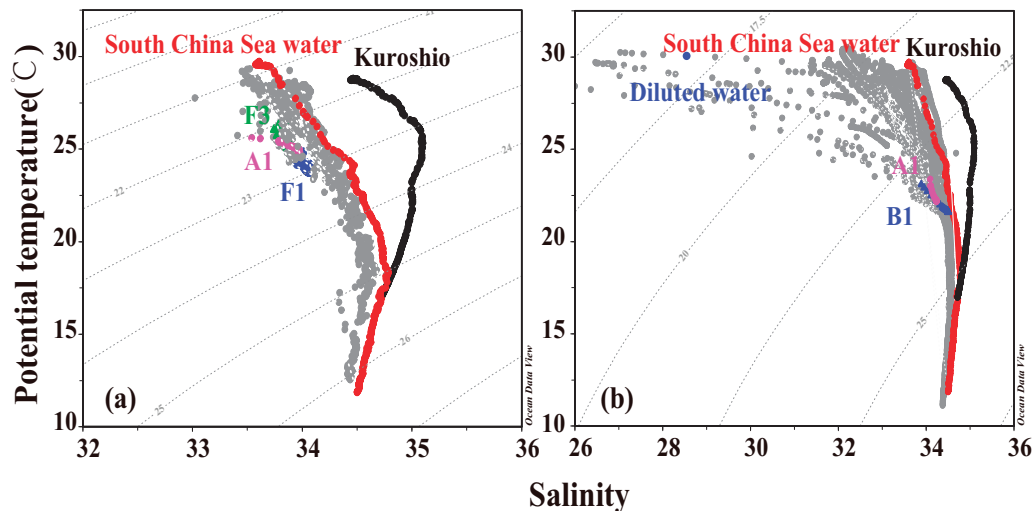
Figure 4. Temperature–salinity (T–S) diagram of water samples during summer cruises of 2004 (a) and 2005 (b). The black (solid) and red lines (open circles) represent the Kuroshio water and South China Sea water respectively. The green, pink, and blue dots (dots marked with names) in Figure 4a represent the water at Stns. F3, A1, and F1 during the 2004 cruise, whereas the pink and blue dots in Figure 4b represent the water at Stns. A1 and B1 during the 2005 cruise.

We used GAMs to explain the effect of temperature and nutrients on diatoms and *Synechococcus* (Figure 10b). Diatoms seemed to adapt to a relatively wide temperature range. They reached a peak biomass in the temperature range of 22–26°C and became less abundant when the temperature exceeded 26°C. Diatom abundance also correlated strongly and positively with silicate concentrations and Si:N ratios, as opposed to *Synechococcus*, which increased in abundance when temperature increased and silicate and NO_x concentrations decreased.

Discussion
Factors influencing phytoplankton composition in the different stages of an upwelling event

The three distinct stages of upwelling could be distinguished from the hydrological, chemical, and biological characteristics of the upwelled water and corresponded to previously described stages (Brown and Hutchings, 1987; Mohrholz *et al.*, 2014). Analysis of the three stages showed how dramatic changes in nutrient availability and temperature impacted the plankton community during upwelling. In some ways how the different stages of upwelling impacted the phytoplankton was analogous to the effects of changes in physics, chemistry, and biology on phytoplankton biomass and community structure during the life cycle of a cyclonic eddy (Sweeney *et al.*, 2003; Coria-Monter *et al.*, 2014). However, the intermittent nature of upwelling make environmental conditions more complex and lead to stochastic, short-term variations of the phytoplankton community (Vidal *et al.*, 2017). It is well known that diatoms dominate in the first two stages of any upwelling in the EBCUS, whereas dinoflagellates, which have a different niche with respect to temperature and nutrient conditions (Margalef, 1978; Guo *et al.*, 2014), flourish in stable and stratified environments with low nutrient concentrations (Brown and Hutchings, 1987; Hansen *et al.*, 2014). Our results showed that diatoms dominated in the first two stages of upwelling, but dinoflagellates were always present in low concentrations, and instead there were marked increases of *Synechococcus* biomass during the third stage of upwelling. The

RDA analyses indicated that diatoms and *Synechococcus*, which dominated the changes of the phytoplankton community, were influenced by different environmental factors (Figure 10a). In the following sections, we examine the factors that potentially accounted for the short-term changes of the phytoplankton community.

Diatoms, aloricate ciliates, and tintinnids dominated in the first stage of upwelling

The high nutrient concentrations, low temperatures, and vertical mixing that characterized the first two stages of upwelling resulted in a diatom-dominated phytoplankton community in line with observations of the mature upwelled water off Namibia (Hansen *et al.*, 2014). Silva *et al.* (2009) have reported that small, chain-forming, and colonial diatoms such as *T. nitzschioides* and *L. danicus* respond quickly to upwelling and dominate the phytoplankton community in the first stage of upwelling.

Several factors may account for the dominance of diatoms during the first two stages of upwelling (Figure 8). First, diatoms have a "low-SST, low-irradiance, high nutrient niche" (Irwin *et al.*, 2012), which fits well with conditions in the early stage of upwelling, as is also demonstrated using the GAMs model (Figure 10b). Diatoms grow well when nutrient concentrations are relatively high and temperatures are low (21–26°C). Second, relatively large phytoplankton can react more rapidly and uptake nutrients longer than small phytoplankton (Fawcett and Ward, 2011). The vacuole of diatoms gives them a large capacity to store nutrients (Thingstad *et al.*, 2005) and a competitive advantage over other phytoplankton in using recently upwelled nutrients, especially nitrate (Sarthou *et al.*, 2005; Liu *et al.*, 2016). However, because of their siliceous frustules, diatoms are more dependent on silicate concentrations, and diatom biomass is not surprisingly correlated positively with silicate concentrations (Figure 10b). Diatoms have a relatively high growth rate compared with dinoflagellates and cyanobacteria at low temperatures (Chen and Laws, 2017), and thus the mean surface temperatures in the first two stages, 21–25°C, were well suited for diatom growth
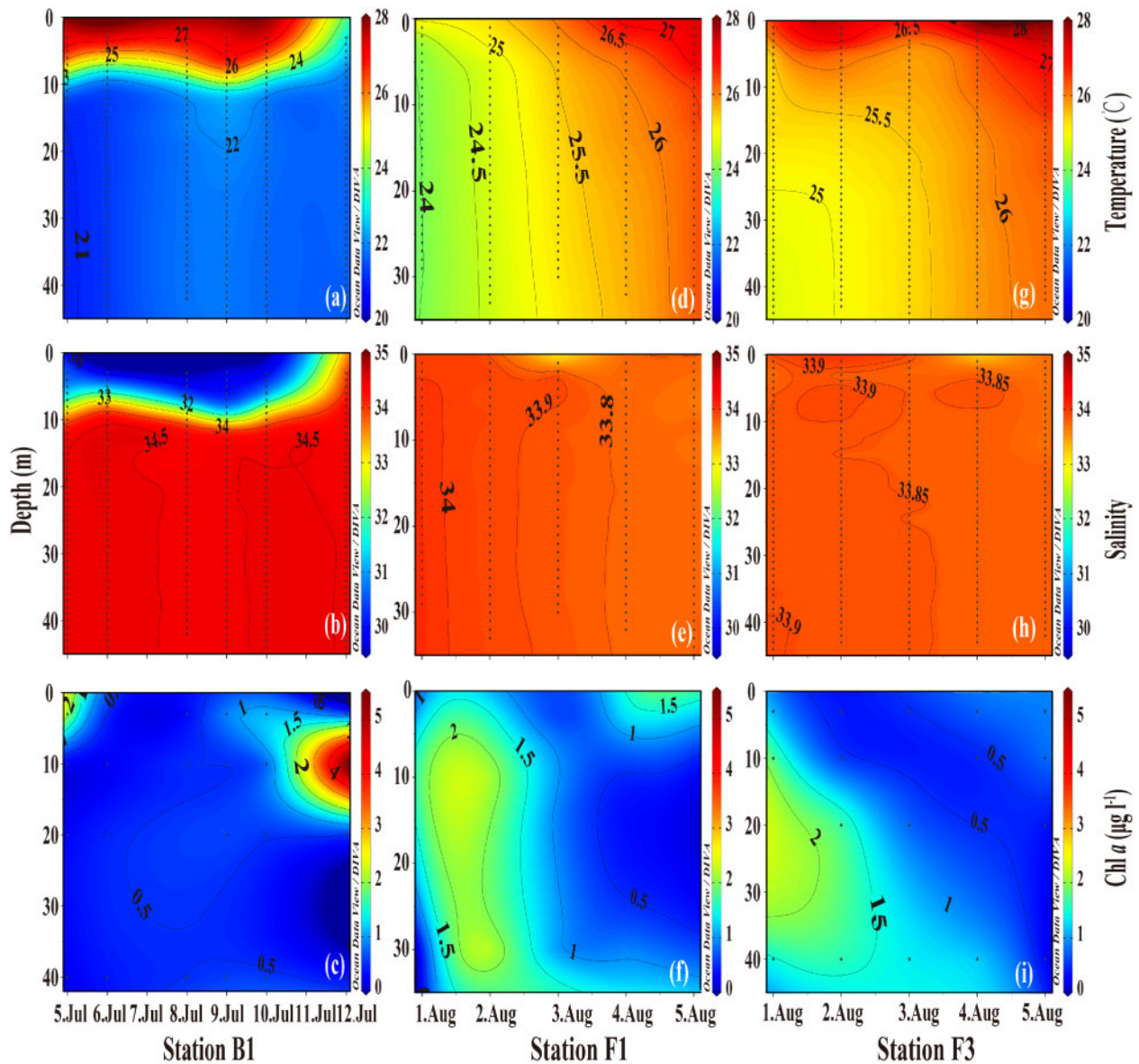
Figure 5. Temporal changes of temperature (°C, upper panels, a, d, g), salinity (middle panels, b, e, h), and total Chl *a* (μg l^{-1}, bottom panels, c, f, i) of Stns. B1 (left), F1 (middle), and F3 (right).

(Figure 10b). The suitability of similar temperatures for diatom growth has previously been demonstrated in the ECS (Liu *et al.*, 2016). Third, during the early stages of upwelling, the dominant species are relatively large cells or chain-forming diatoms such as *S. costatum* and *Thalassionema*, which are adapted to highly turbulent, upwelled water (Tilstone *et al.*, 2000), and are not good prey for microzooplankton. At the initiation of upwelling, aloricate ciliates and tintinnids dominated the microzooplankton community (Figure 9a), and microzooplankton abundance and grazing in the surface were constrained by the relatively low phytoplankton biomass. Because of their small sizes, tintinnids graze mainly on pico- and nano-phytoplankton, and during the first stage of upwelling, microzooplankton grazing exerted little control on the diatom bloom.

As the upwelled water aged, diatom biomass and growth rates decreased because of the low nutrient concentrations and the reduced Si:N ratio. Taxa that are known to suffer from phosphorus

deficiency include *T. nitzschioides* and *P. pungens* (Ou *et al.*, 2006). The decrease of *Skeletonema* and *Leptocylindrus* abundance more likely resulted from the low Si:N ratios (Anabalón *et al.*, 2016).

Synechococcus and heterotrophic dinoflagellates increased as the upwelled water aged

As the upwelling weakened, nutrient concentrations decreased, the temperature increased, and the contributions of *Synechococcus* to the total Chl *a* increased. This increase of *Synechococcus* abundance contrasts with the findings in other upwelling systems where the phytoplankton composition shifts from diatoms to dinoflagellates (Mitchell-Innes and Walker, 1991). The dinoflagellate biomass remained low throughout our observations. The explanation may be that dinoflagellates have a poor tolerance to changes of temperature and nutrients and that
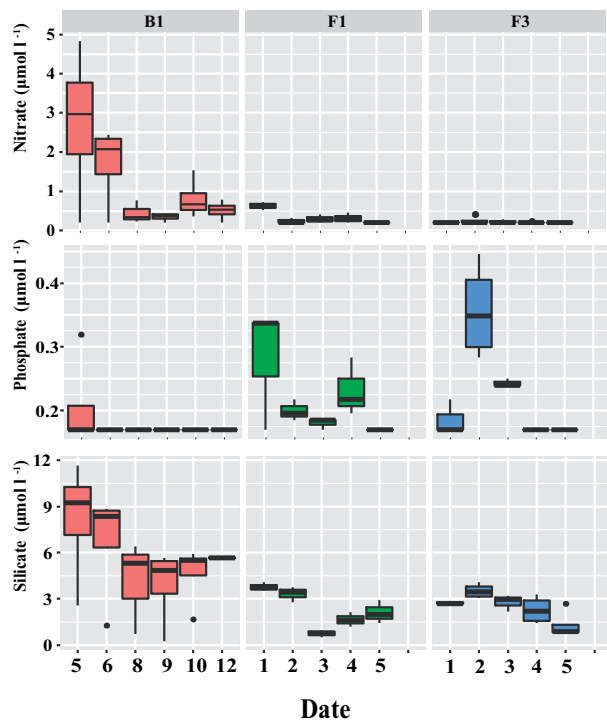
Figure 6. The boxplots of all nutrients samples throughout the water column at Stns. B1, F1, and F3 for nitrate (upper), phosphate (middle), and silicate (bottom) during the observation periods. The bottom of the box represents the lower 25% of our data (the lower quartile), the top of the box represents the upper 25% of our data (the upper quartile), and the bold black line in the box represents the median value of our data. The whiskers are defined as 1.5 times the inter-quartile range, and the dots outside the whiskers are considered as outliers. Red (right) boxplots represent the nutrients in the water column of Stn. B1 during 5–12 July 2005 (July 5, 6, 8, 9, 10, and 12); green (middle) boxplots represent the nutrients in the water column of Stn. F1 during 1–5 August 2004 (August 1, 2, 3, 4, and 5); and blue (left) boxplots represent the nutrients in the water column of Stn. F3 during 1–5 August 2004 (August 1, 2, 3, 4, and 5).

Figure 7. Cluster analysis for the four stations (B1, F1, F3, A1) based on the surface temperature, salinity, oxygen, nitrate, and Chl *a* concentrations (B1b-5, B1b-6, B1b-8, B1b-9, B1b-10, and B1b-12) were presented the time-series observation of Stn. B1 during 5–12 July 2005; A1a-29 and A1b-14 were presented the survey of Stn. A1 on 29 July 2004 and 14 July 2005 respectively; F1a-1, F1a-2, F1a-3, F1a-4, and F1a-5 were represented for the time-series investigation at Stn. F1 during 1–5 August 2004; F3a-1, F3a-2, F3a-3, F3a-4, and F3a-5 were represented for the time-series investigation at Stn. F3 during 1–5 August 2004; The *K* value was used to select the right number of clusters using the function NbClust based on the distance between samples in the "Cluster" packages in R. The clusters represented by red boxes resulted from the *K* value.

they have "relatively low temperature and high nutrient niches", compared with *Synechococcus* (Chavez *et al.*, 1991; Silva *et al.*, 2009; Xiao *et al.*, 2018b). Dinoflagellate biomass reaches a maximum when the temperature is ∼19°C (Liu *et al.*, 2016), and they therefore often bloom in late spring in the ECS. In the current study areas, the temperatures increased with the phase of upwelling and eventually reached more than 28°C (Figure 5), which is too high for most dinoflagellates. Dinoflagellates can mobilize alkaline phosphatase to use organic phosphorus when phosphate concentrations are low (Ou *et al.*, 2006), but they are relatively sensitive to low nitrate concentrations and prefer high N:P ratios. In the ECS, concentrations of peridinin, which is the diagnostic pigment for dinoflagellates, are high when phosphorus has been consumed ($<0.1\,\mu mol\,l^{-1}$) and NO_X concentrations are relatively high ($>0.5\,\mu mol\,l^{-1}$; Xiao *et al.*, 2018a). At the end of upwelling in the STWS, nitrate and phosphate concentrations were below the detection limits, indicating that dinoflagellate growth was limited by nitrate.

Synechococcus is, as opposed to the dinoflagellates, related to a higher temperature and lower nutrient niche (Xiao *et al.*, 2018b). *Synechococcus* often thrives at relatively high temperatures

(Moisan *et al.*, 2010). The almost linear increase of *Synechococcus* biomass with increased temperature in the lower temperature range and high biomass at temperatures >27°C was therefore not unexpected (Figure 10b). In fact, this pattern is rather consistent with observations from the NW Mediterranean Sea and southern Mid-Atlantic Bight, where *Synechococcus* abundance exhibits a seasonal pattern, and the highest abundance occurs during the warm season (Agawin *et al.*, 1998; Moisan *et al.*, 2010). In addition to the direct effect of temperature, the high *Synechococcus* biomass at high temperature is also affected by the relationship between temperature and nutrient concentrations. Temperature is usually negatively correlated with nutrient availability in low nutrient waters. Under nutrient-depleted conditions, *Synechococcus* competes well for nutrients because of its relatively large surface-to-volume ratio (Moisan *et al.*, 2010). It therefore plays an important role in areas such as eddies, offshore jets, and river plumes (Chen *et al.*, 2009). The increase of ammonium concentrations as nitrate concentrations decreased in the aged water probably favours picoplankton growth in general (Joint *et al.*, 2001).

Phytoplankton succession is related not only to bottom-up control but also to the microzooplankton community and its grazing activity. The selectivity of microzooplankton grazing is dramatically affected by the composition of the

Table 1. The surface temperature, salinity, dissolved oxygen (DO), nitrate, and Chl *a* concentrations during the three stages of upwelling evolution based on time-series investigations of the four stations (Stns. B1, F1, F3, and A1) in the southern Taiwan Strait.

Group	Station	Date	Temperature (°C)	Salinity	Chl *a* (μg l^{-1})	DO (mg l^{-1})	nitrate (μmol l^{-1})
Stage 1-upwelling	A1	14 July 2005	24.18	34.05	0.90	6.85	0.20
	B1	12 July 2005	23.08	33.89	1.44	7.10	0.20
	Mean		23.63	33.97	1.17	6.97	0.20
Stage 2-upwelling	A1	29 July 2004	25.30	33.71	0.74	8.23	0.82
	F1	1 August 2004	24.78	33.99	2.04	8.07	0.52
	Mean		25.04	33.85	1.39	8.15	0.67
Stage 3-upwelling	F2	2 August 2004	25.25	33.93	1.51	8.83	0.10
	F3	3 August 2004	25.98	33.43	1.13	8.67	0.27
	F4	4 August 2004	26.95	33.76	1.38	8.77	0.13
	F5	5 August 2004	27.36	33.78	0.87	8.62	0.10
	F3	1 August 2004	26.35	33.86	0.87	9.05	0.10
	F3	2 August 2004	27.33	33.98	0.45	8.82	0.12
	F3	3 August 2004	26.64	33.88	0.39	8.86	0.09
	F3	4 August 2004	27.69	33.43	0.35	8.83	0.09
	F3	5 August 2004	27.83	33.73	0.25	8.79	0.12
	Mean		26.82	33.75	0.80	8.80	0.13
Plume	B1	5 July 2005	27.20	30.65	0.87	8.20	0.20
	B1	6 July 2005	27.28	29.87	0.99	8.47	0.20
	B1	8 July 2005	27.03	29.53	1.96	8.11	0.23
	B1	9 July 2005	27.25	29.79	1.95	7.74	0.20
	B1	10 July 2005	27.37	29.90	2.04	7.10	0.36
	Mean		27.23	29.95	1.56	7.92	0.24
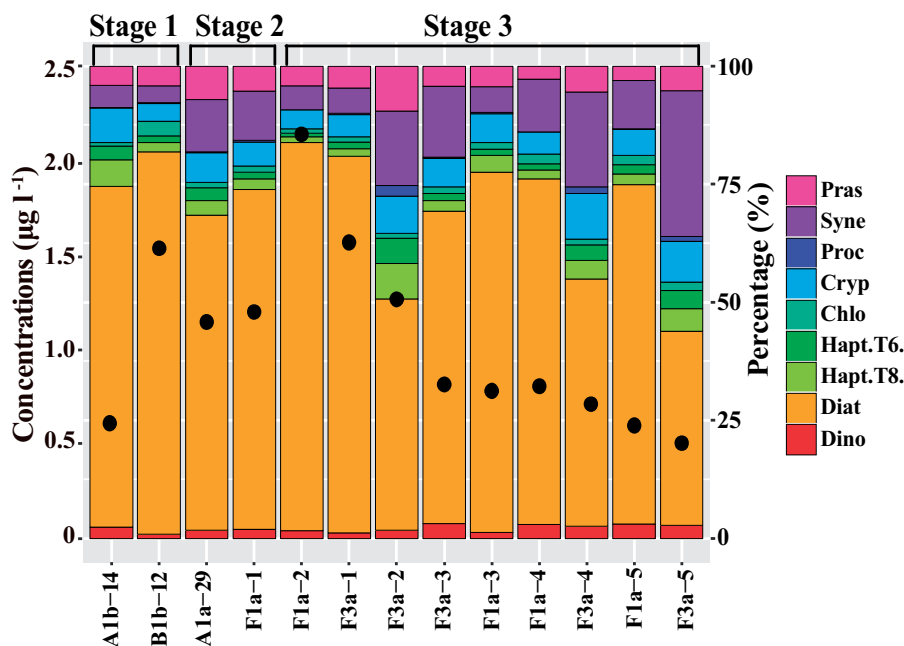
Figure 8. Dynamic of the averaged depth-integrated phytoplankton biomass and community composition based on the HPLC pigments analysis during the different stages of upwelling in the southern Taiwan Strait (see Figure 7 for sample names of *x*-axis). The black dots are the Chl *a* concentrations as a proxy for biomass, corresponding to the *y*-axis on the right, and the coloured bars are the percentage values corresponding to the *y*-axis on the left. Abbreviations: Dino, dinoflagellates; Diat, diatoms; Hapt.T8., haptophytes (Type 8); Hapt.T6., haptophytes (Type 6); Chlo, chlorophytes; Cryp, cryptophytes; Proc, *Prochlorococcus*; Syne, *Synechococcus*; Pras, prasinophytes.

microzooplankton, which is determined by the characteristics of the prey (phytoplankton biomass, size, and nutrient content) and other factors such as abiotic environmental factors (e.g. temperature, light) and predator populations (Sun *et al.*, 2007). In coastal waters, a large proportion of microzooplankton is accounted for by large aloricate ciliates and tintinnids, which prefer to graze on

10–30 μm size phytoplankton such as diatoms, cryptophytes, and autotrophic dinoflagellates (Strom *et al.*, 2001). Large phytoplankton can also be grazed effectively by heterotrophic dinoflagellates, which can compete with copepods for large prey such as diatoms, and especially for large heterotrophic dinoflagellates such as *Gymnodinium* spp., which have relatively short generation
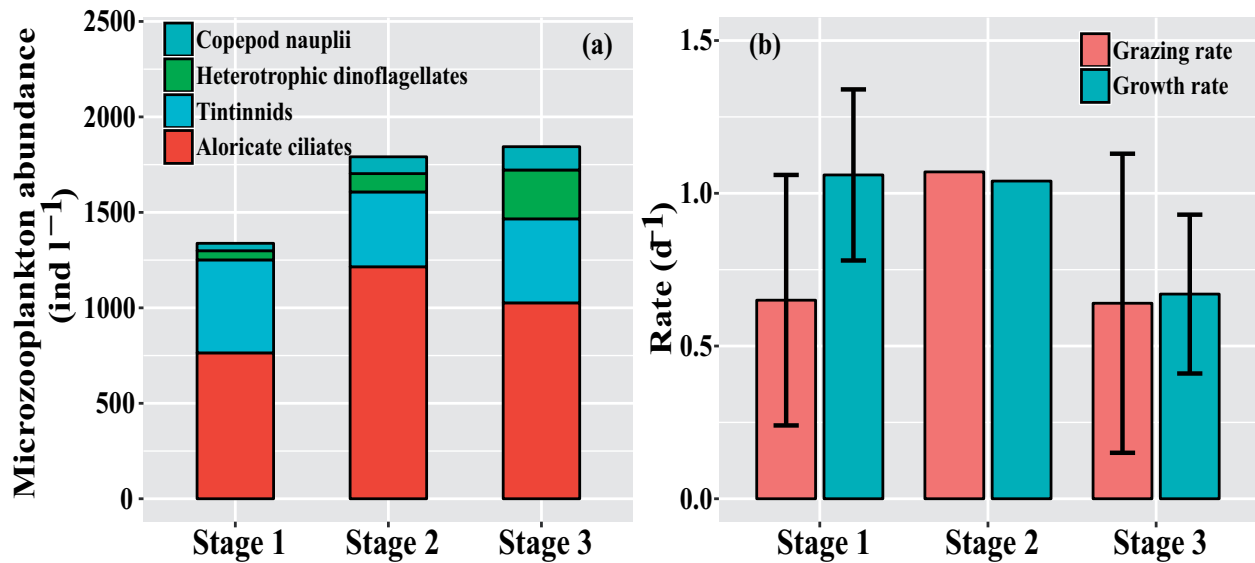
Figure 9. The averaged depth-integrated microzooplankton abundance and composition (a); surface phytoplankton growth rate and microzooplankton grazing rate (b) at the different stages of upwelling in the southern Taiwan Strait. The error bars represent the standard deviations and there were only two surface phytoplankton growth rates and microzooplankton grazing rates in the second stage of upwelling.
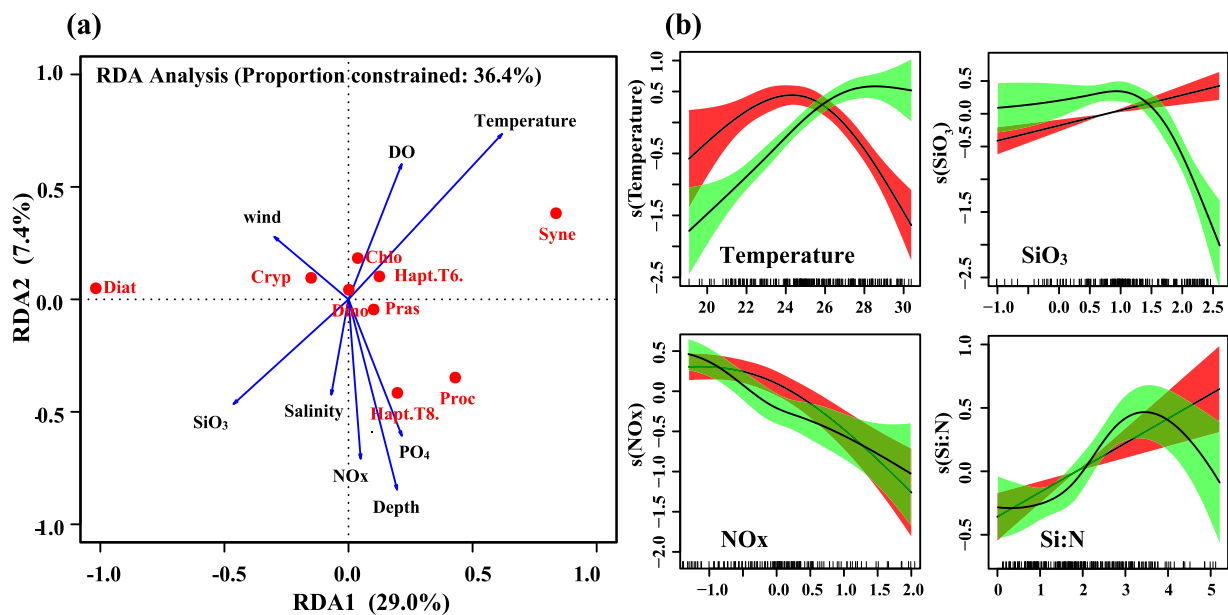
Figure 10. Redundancy analysis for the relationships between phytoplankton community and environmental factors in the southern Taiwan Strait during summer cruises of 2004 and 2005 (a) Blue axes (arrows) represent the environmental factors, whereas red circles represent the phytoplankton groups. Variables are: temperature, salinity, nitrate+ nitrite (NO_x), phosphate (PO_4), silicate (SiO_3), wind (monthly mean windspeeds). Results of generalized additive models (GAMs) presenting diatom (red; dark grey) and *Synechococcus* (green; light grey) with temperature, nitrate+ nitrite, silicate, and Si:N in the STWS (b). Nutrient concentrations are natural logarithm transformed. Solid lines represent smoothed mean relationships from GAMs and shaded areas are 95% confidence intervals.

times and respond rapidly to an increase of prey abundance (Hansen, 1992; Neuer and Cowles, 1994; Sherr and Sherr, 2007). In the current study, the abundance of aloricate ciliates and heterotrophic dinoflagellates increased during the second stage as upwelling weakened (Figure 9a), and grazing then exerted strong top-down control on the abundance of diatoms and thereby influenced phytoplankton biomass and composition. Similar results have also been reported during the relaxation phase of

upwelling off the Galician Coast, where the measured microzooplankton grazing rates exceeded phytoplankton growth rates (Fileman and Burkill, 2001). Guo *et al.* (2011) have found that during the STWS upwelling period, copepod abundance is strongly correlated with Chl *a* concentrations, and the grazing pressure that copepods exert on phytoplankton is higher in upwelling areas than in non-upwelling areas. Some studies have also shown that the feeding by mesozooplankton such as copepods
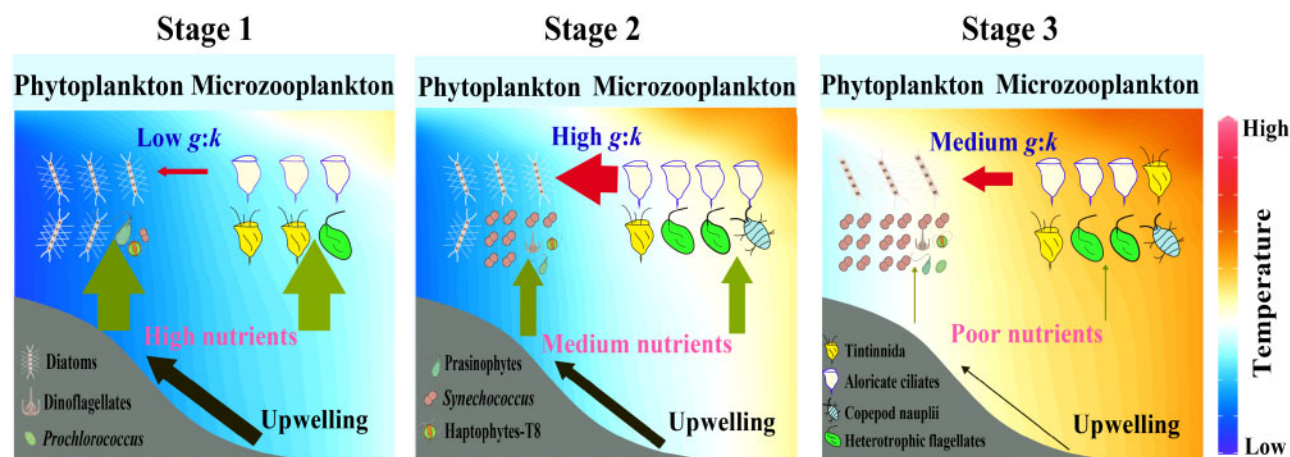
Figure 11. Schematic diagram of the changes in temperature and nutrient concentrations and plankton community during the different stages of coastal upwelling ecosystems. Black, green, and red arrows represent the upwelling intensity, the input of nutrient concentrations and the pressure of microzooplankton grazing activity respectively.

seems to be higher at the end of a phytoplankton bloom than in mature upwelled water (Painting *et al.*, 1993; Slaughter *et al.*, 2006). The implication is that mesozooplankton grazing is an important cause of changes in phytoplankton biomass during the relaxation of upwelling.

Changes of the phytoplankton community composition during the upwelling events could therefore be attributed to the ways different phytoplankton groups responded to changes of temperature and nutrient concentrations and were impacted by zooplankton grazing.

Effects of the Pearl River plume on the phytoplankton community during upwelling events

The hydrological conditions in the STWS are quite complex because the wind, currents, and bottom topography are all variable (Hong *et al.*, 2011). Five major water masses have been identified in this area during summer (Hu *et al.*, 2011). The horizontal distributions of surface temperature and salinity revealed that this area is impacted by a combination of waters from the SCS and the plume from the Pearl River (Figure 4).

Notably, the effects of the Pearl River plume and coastal upwelling are interactive in the STWS, and the interactions play an important role in enhancing phytoplankton biomass and sustaining high primary production (Gan *et al.*, 2009b; Liu *et al.*, 2011). Several studies have confirmed that the Pearl River plume can extend into the STWS as far as the Penghu Channel when the Pearl River discharge is large and southwesterly winds are strong (Bai *et al.*, 2015; Chen *et al.*, 2017a, b). The association between the movement of the Pearl River plume and the development of upwelling, which can influence the plume's trajectory, dynamics, and fresh-water transport (Chen *et al.*, 2017a, b), is consistent with our findings. At the start of continuous observations at Stn. B1, warm, low-salinity water covered the surface, and cold, saline water was found only below a depth of 10 m. The low-salinity water subsequently disappeared as upwelling progressed. Nutrient concentrations in the plume were sufficient to cause high biological productivity in the northern SCS (Gan *et al.*, 2010), but at the edge of the plume, co-limitation by phosphorus and silicate (Yin *et al.*, 2001) depressed phytoplankton growth. That co-limitation is probably the reason why the surface phytoplankton biomass

was lower at Stn. B1 during 6–9 July than on 5 July. The atomic N:P ratios were high ($>$100) in the Pearl River plume and low ($\sim$10) in the upwelled water. The combination of excess nitrogen in the plume water with surplus phosphorus from the upwelled water therefore promoted phytoplankton growth (Harrison *et al.*, 2008). However, the impact of the interactions between the plume and upwelling on the plankton community, including both the phytoplankton and microzooplankton community, is still unclear, especially in the STWS. The River Influences on Shelf Ecosystems programme, which focused on the coastal waters of the northeast Pacific Ocean, has been the only comprehensive study of the ecosystem dynamics associated with the coupling between a river plume and coastal upwelling (Frame and Lessard, 2009; Hickey *et al.*, 2010). More studies focused on the interactions between estuarine plumes and coastal upwelling are needed to better understand these systems.

Summary

Time-series investigations carried out as a part of this study in the STWS revealed three stages of upwelling (recently upwelled water, mature water, and aged water) based on surface temperature, salinity, and concentrations of oxygen, nitrate, and Chl *a*. We found that during pulsed upwelling events, there were changes not only in temperature and nutrient concentrations, but also in the entire phytoplankton and microzooplankton communities (Figure 11). The results showed that phytoplankton reacted rapidly to the nutrients supplied at the initiation of upwelling and grew rapidly during the first two stages. Diatoms dominated the phytoplankton community in the first two stages. As the intensity of upwelling decreased, there was a clear increase in the contributions of *Synechococcus* to the Chl *a*. Aloricate ciliates and tintinnids dominated the microzooplankton community during upwelling, and the average depth-integrated abundance of microzooplankton and heterotrophic dinoflagellates increased as upwelling weakened. Microzooplankton grazing on phytoplankton reached a maximum during the second stage and roughly balanced phytoplankton growth in the third stage. Our findings suggest that phytoplankton succession is a response to the changes of temperature and nutrient concentrations during upwelling, and that response can explain to a large extent the shift from a

diatom-dominated to a *Synechococcus*-dominated phytoplankton community. Changes within the microzooplankton community and microzooplankton grazing activity were also important factors that induced shifts of phytoplankton composition.

The interactions between the Pearl River plume and upwelling in the coastal areas added complexity to the STWS ecosystem and led to changes of physicochemical and biological factors during the southwestern monsoon. Deeper understanding of the mechanisms of how plankton communities are influenced by the coupling of river plumes and upwelling in coastal areas will require further investigations, including *in situ* tracking surveys and numerical modelling analysis.

Supplementary data

Supplementary material is available at the *ICESJMS* online version of the manuscript.

Acknowledgements

References

Agawin, N. S. R., Duarte, C. M., and Agustí, S. 1998. Growth and abundance of *Synechococcus* sp. in a Mediterranean Bay: seasonality and relationship with temperature. Marine Ecology Progress Series, 170: 45–53.

Anabalón, V., Morales, C. E., González, H. E., Menschel, E., Schneider, W., Hormazabal, S., and Valencia, L. 2016. Micro-phytoplankton community structure in the coastal upwelling zone off Concepción (central Chile): annual and inter-annual fluctuations in a highly dynamic environment. Progress in Oceanography, 149: 174–188.

Bai, Y., Huang, T. H., He, X., Wang, S. L., Hsin, Y. C., Wu, C. R., Zhai, W. *et al.* 2015. Intrusion of the Pearl River plume into the main channel of the Taiwan Strait in summer. Journal of Sea Research, 95: 1–15.

Brown, P. C., and Hutchings, L. 1987. The development and decline of phytoplankton blooms in the southern Benguela upwelling system. 1. Drogue movements, hydrography and bloom development. South African Journal of Marine Science, 5: 357–391.

Chapman, P., and Bailey, G. W. 1991. Short-term variability during an anchor station study in the southern Benguela upwelling system: introduction. Progress in Oceanography, 28: 1–152.

Chavez, F. P., Barber, R. T., Kosro, P. M., Huyer, A., Ramp, S. R., Stanton, T. P., and Mendiola, B. R. D. 1991. Horizontal transport and the distribution of nutrients in the coastal transition zone off northern California: effects on primary production, phytoplankton biomass and species composition. Journal of Geophysical Research Oceans, 96: 14833–14848.

Chen, B., and Laws, E. A. 2017. Is there a difference of temperature sensitivity between marine phytoplankton and heterotrophs? Limnology and Oceanography, 62: 806–817.

Chen, B., Liu, H., Landry, M. R., Dai, M., Huang, B., and Sune, J. 2009. Close coupling between phytoplankton growth and

microzooplankton grazing in the western South China Sea. Limnology and Oceanography, 54: 1084–1097.

Chen, Z., Jiang, Y., Liu, J. T., and Gong, W. 2017a. Development of upwelling on pathway and freshwater transport of Pearl River plume in northeastern South China Sea. Journal of Geophysical Research Oceans, 122: 6090–6109.

Chen, Z., Pan, J., Jiang, Y., and Lin, H. 2017b. Far-reaching transport of Pearl River plume water by upwelling jet in the northeastern South China Sea. Journal of Marine Systems, 173: 60–69.

Core, T. R. 2014. A Language and Environment for Statistical Computing. R Foundation for Statistical Computing, Vienna, Austria.

Coria-Monter, E., Monreal-Gómez, M. A., Salas-de-León, D. A., Javier, A-R., and Merino-Ibarra, M. 2014. Differential distribution of diatoms and dinoflagellates in a cyclonic eddy confined in the bay of La Paz, Gulf of California. Journal of Geophysical Research: Oceans, 119: 6258–6268.

Du, X., and Peterson, W. T. 2013. Seasonal cycle of phytoplankton community composition in the coastal upwelling system off central Oregon in 2009. Estuaries and Coasts, 37: 299–311.

Fawcett, S. E., and Ward, B. B. 2011. Phytoplankton succession and nitrogen utilization during the development of an upwelling bloom. Marine Ecology Progress Series, 428: 13–31.

Field, C. B., Behrenfeld, M. J., Randerson, J. T., and Falkowski, P. 1998. Primary production of the biosphere: integrating terrestrial and oceanic components. Science, 281: 237–240.

Fileman, E., and Burkill, P. 2001. The herbivorous impact of microzooplankton during two short-term Lagrangian experiments off the NW coast of Galicia in summer 1998. Progress in Oceanography, 51: 361–382.

Fréon, P., Barange, M., and Arístegui, J. 2009. Eastern boundary upwelling ecosystems: integrative and comparative approaches. Progress in Oceanography, 83: 1–14.

Frame, E. R., and Lessard, E. J. 2009. Does the Columbia River plume influence phytoplankton community structure along the Washington and Oregon coasts? Journal of Geophysical Research Oceans, 114: C00B09.

Gan, J., Cheung, A., Guo, X., and Li, L. 2009a. Intensified upwelling over a widened shelf in the northeastern South China Sea. Journal of Geophysical Research, 114: C09019.

Gan, J., Li, L., Wang, D., and Guo, X. 2009b. Interaction of a river plume with coastal upwelling in the northeastern South China Sea. Continental Shelf Research, 29: 728–740.

Gan, J., Lu, Z., Dai, M., Cheung, A. Y. Y., Liu, H., and Harrison, P. 2010. Biological response to intensified upwelling and to a river plume in the northeastern South China Sea: a modeling study. Journal of Geophysical Research Oceans, 115: C09001.

Grime, J. P. 1977. Evidence for the existence of three primary strategies in plants and its relevance to ecological and evolutionary theory. The American Naturalist, 111: 1169–1194.

Guo, D. H., Huang, J. Q., and Li, S. J. 2011. Planktonic copepod compositions and their relationships with water masses in the southern Taiwan Strait during the summer upwelling period. Continental Shelf Research, 31: 67–76.

Guo, S., Feng, Y., Wang, L., Dai, M., Liu, Z., Bai, Y., and Sun, J. 2014. Seasonal variation in the phytoplankton community of a continental-shelf sea: the East China Sea. Marine Ecology Progress Series, 516: 103–126.

Hansen, A., Ohde, T., and Wasmund, N. 2014. Succession of micro- and nanoplankton groups in ageing upwelled waters off Namibia. Journal of Marine Systems, 140: 130–137.

Hansen, P. J. 1992. Prey size selection, feeding rates and growth dynamics of heterotrophic dinoflagellates with special emphasis on *Gyrodinium spirale*. Marine Biology, 114: 327–334.

Harrison, P. J., Yin, K., Lee, J. H. W., Gan, J., and Liu, H. 2008. Physical–biological coupling in the Pearl River estuary. Continental Shelf Research, 28: 1405–1415.

Hickey, B. M., Kudela, R. M., Nash, J. D., Bruland, K. W., Peterson, W. T., MacCready, P., Lessard, E. J. et al. 2010. River influences on shelf ecosystems: introduction and synthesis. Journal of Geophysical Research, 115: C00B17.

Hong, H., Chai, F., Zhang, C., Huang, B., Jiang, Y., and Hu, J. 2011. An overview of physical and biogeochemical processes and ecosystem dynamics in the Taiwan Strait. Continental Shelf Research, 31: 3–12.

Hong, H., Zhang, C., Shang, S., Huang, B., Li, Y., Li, X., and Zhang, S. 2009. Interannual variability of summer coastal upwelling in the Taiwan Strait. Continental Shelf Research, 29: 479–484.

Hu, J., Hong, H., Li, Y., Jiang, Y., Chen, Z., Zhu, J., Wan, Z. et al. 2011. Variable temperature, salinity and water mass structures in the southwestern Taiwan Strait in summer. Continental Shelf Research, 31: 13–23.

Hu, J., Lan, W., Huang, B., Chiang, K., and Hong, H. 2015. Low nutrient and high chlorophyll *a* coastal upwelling system—a case study in the southern Taiwan Strait. Estuarine, Coastal and Shelf Science, 166: 170–177.

Huang, B., Xiang, W., Zeng, X., Chiang, K., Tian, H., Hu, J., Lan, W. et al. 2011. Phytoplankton growth and microzooplankton grazing in a subtropical coastal upwelling system in the Taiwan Strait. Continental Shelf Research, 31: 48–56.

Irwin, A. J., Nelles, A. M., and Finkel, Z. V. 2012. Phytoplankton niches estimated from field data. Limnology and Oceanography, 57: 787–797.

Jing, Z., Qi, Y., Hua, Z., and Zhang, H. 2009. Numerical study on the summer upwelling system in the northern continental shelf of the South China Sea. Continental Shelf Research, 29: 467–478.

Joint, I., Rees, A. P., and Woodward, E. M. S. 2001. Primary production and nutrient assimilation in the Iberian upwelling in August 1998. Progress in Oceanography, 51: 303–320.

Landry, M. R., Kirshtein, J., and Constantinou, J. 1995. A refined dilution technique for measuring the community grazing impact of microzooplankton, with experimental tests in the central equatorial Pacific. Marine Ecology Progress Series, 120: 53–63.

Lips, I., and Lips, U. 2010. Phytoplankton dynamics affected by the coastal upwelling events in the Gulf of Finland in July–August 2006. Journal of Plankton Research, 32: 1269–1282.

Litchman, E., Edwards, K. F., Klausmeier, C. A., and Thomas, M. K. 2012. Phytoplankton niches, traits and eco-evolutionary responses to global environmental change. Marine Ecology Progress Series, 470: 235–248.

Liu, H., Song, X., Huang, L., Tan, Y., and Zhang, J. 2011. Phytoplankton biomass and production in northern South China Sea during summer: influenced by Pearl River discharge and coastal upwelling. Acta Ecologica Sinica, 31: 133–136.

Liu, X., Xiao, W., Landry, M. R., Chiang, K., Wang, L., and Huang, B. 2016. Responses of phytoplankton communities to environmental variability in the East China Sea. Ecosystems, 19: 832–849.

Mackey, M., Mackey, D., Higgins, H., and Wright, S. 1996. CHEMTAX—a program for estimating class abundances from chemical markers: application to HPLC measurements of phytoplankton. Marine Ecology Progress Series, 144: 265–283.

Margalef, R. 1978. Life-forms of phytoplankton as survival alternatives in an unstable environment. Oceanologica Acta, 1: 493–509.

Mitchell-Innes, B. A., and Walker, D. R. 1991. Short-term variability during an anchor station study in the southern Benguela upwelling system: phytoplankton production and biomass in relation to specie changes. Progress in Oceanography, 28: 65–89.

Mohrholz, V., Eggert, A., Junker, T., Nausch, G., Ohde, T., and Schmidt, M. 2014. Cross shelf hydrographic and hydrochemical conditions and their short term variability at the northern Benguela during a normal upwelling season. Journal of Marine Systems, 140: 92–110.

Moisan, T. A., Blattner, K. L., and Makinen, C. P. 2010. Influences of temperature and nutrients on *Synechococcus* abundance and biomass in the southern Mid-Atlantic Bight. Continental Shelf Research, 30: 1275–1282.

Neuer, S., and Cowles, T. J. 1994. Protist herbivory in the Oregon upwelling system. Marine Ecology Progress Series, 113: 147–162.

Oh, H. J., Suh, Y. S., and Heo, S. 2004. The relationship between phytoplankton distribution and environmental conditions of the upwelling cold water in the eastern coast of the Korean Peninsula. Journal of the Korean Association of Geographic Information Studies, 7: 166–173.

Ou, L., Huang, B., Lin, L., Hong, H., Zhang, F., and Chen, Z. 2006. Phosphorus stress of phytoplankton in the Taiwan Strait determined by bulk and single-cell alkaline phosphatase activity assays. Marine Ecology Progress Series, 327: 95–106.

Pai, S. C., Yang, C. C., and Riley, J. P. 1990a. Effects of acidity and molybdate concentration on the kinetics of the formation of the phosphoantimonylmolybdenum blue complex. Analytica Chimica Acta, 229: 115–120.

Pai, S. C., Yang, C. C., and Riley, J. P. 1990b. Formation kinetics of the pink azo dye in the determination of nitrite in natural waters. Analytica Chimica Acta, 232: 345–349.

Painting, S. J., Lucas, M. I., Peterson, W. T., Brown, P. C., Hutchings, L., and Mitchell, I., B. A. 1993. Dynamics of bacterioplankton, phytoplankton and mesozooplankton communities during the development of an upwelling plume in the southern Benguela. Marine Ecology Progress Series, 100: 35–53.

Parsons, T. R. 1984. A manual of chemical and biological methods for seawater analysis. Deep Sea Research Part A Oceanographic Research Papers, 31: 1523.

Pinckney, J. L., Paerl, H. W., Harrington, M. B., and Howe, K. E. 1998. Annual cycles of phytoplankton community-structure and bloom dynamics in the Neuse River estuary, North Carolina. Marine Biology, 131: 371–381.

Reynolds, C. 1984. Phytoplankton periodicity: the interactions of form, function and environmental variability. Freshwater Biology, 14: 111–142.

Sarthou, G., Timmermans, K. R., Blain, S., and Tréguer, P. 2005. Growth physiology and fate of diatoms in the ocean: a review. Journal of Sea Research, 53: 25–42.

Schlitzer, R. 2015. Ocean data view. https://odv.awi.de.

Shang, S. L., Zhang, C. Y., Hong, H. S., Shang, S. P., and Chai, F. 2004. Short-term variability of chlorophyll associated with upwelling events in the Taiwan Strait during the southwest monsoon of 1998. Deep Sea Research Part II: Topical Studies in Oceanography, 51: 1113–1127.

Sherr, E. B., and Sherr, B. F. 2007. Heterotrophic dinoflagellates: a significant component of microzooplankton biomass and major grazers of diatoms in the sea. Marine Ecology Progress Series, 352: 187–197.

Silva, A., Palma, S., Oliveira, P. B., and Moita, M. T. 2009. Composition and interannual variability of phytoplankton in a coastal upwelling region (Lisbon Bay, Portugal). Journal of Sea Research, 62: 238–249.

Slaughter, A. M., Bollens, S. M., and Bollens, G. R. 2006. Grazing impact of mesozooplankton in an upwelling region off northern California, 2000–2003. Deep-Sea Research Part II, 53: 3099–3115.

Strickland, J. D. H., and Parsons, T. R. 1972. A Practical hand book of seawater analysis. Bulletin Fisheries Research Board, Canada. 310 pp.

Strom, S. L., Brainard, M. A., Holmes, J. L., and Olson, M. B. 2001. Phytoplankton blooms are strongly impacted by microzooplankton grazing in coastal North Pacific waters. Marine Biology, 138: 355–368.

Sun, J., Feng, Y., Zhang, Y., and Hutchins, D. A. 2007. Fast microzooplankton grazing on fast-growing, low-biomass phytoplankton: a case study in spring in Chesapeake Bay, Delaware Inland Bays and Delaware Bay. Hydrobiologia, 589: 127–139.

Sweeney, E. N., McGillicuddy, D. J., and Buesseler, K. O. 2003. Biogeochemical impacts due to mesoscale eddy activity in the

Sargasso Sea as measured at the Bermuda Atlantic time-series study (BATS). Deep Sea Research Part II: Topical Studies in Oceanography, 50: 3017–3039.

Takahashi, M., Ishizaka, J., Ishimaru, T., Atkinson, L. P., Lee, T. N., Yamaguchi, Y., Fujita, Y. *et al.* 1986. Temporal change in nutrient concentrations and phytoplankton biomass in short time scale local upwelling around the Izu Peninsula, Japan. Journal of Plankton Research, 8: 1039–1049.

Tang, D. L., Kawamura, H., and Guan, L. 2004. Long-time observation of annual variation of Taiwan Strait upwelling in summer season. Advances in Space Research, 33: 307–312.

Teixeira, I. G., Figueiras, F. G., Crespo, B. G., and Piedracoba, S. 2011. Microzooplankton feeding impact in a coastal upwelling system on the NW Iberian margin: the Ría de Vigo. Estuarine, Coastal and Shelf Science, 91: 110–120.

Thingstad, T. F., Øvreås, L., Egge, J. K., Løvdal, T., and Heldal, M. 2005. Use of non-limiting substrates to increase size; a generic strategy to simultaneously optimize uptake and minimize predation in pelagic osmotrophs? Ecology Letters, 8: 675–682.

Tian, H. 2007. The microzooplankton and its grazing on phytoplankton in typical water of South China Sea. Xiamen University Electronic Theses and Dissertations, pp. 15–27.

Tilstone, G. H., Míguez, B. M., Figueiras, F. G., and Fermín, E. G. 2000. Diatom dynamics in a coastal ecosystem affected by upwelling: coupling between species succession, circulation and biogeochemical processes. Marine Ecology Progress Series, 205: 23–41.

Tomas, C. R. 1997. Identifying Marine Phytoplankton. Academic Press, San Diego. 858 pp.

Utermöhl, H. 1958. Zur Vervollkommnung der quantitativen Phytoplankton-Methodik. Mitteilungen Internationale Vereins Theoretisch Angewiesen Limnologie, 9: 263–272.

Vidal, T., Calado, A. J., Moita, M. T., and Cunha, M. R. 2017. Phytoplankton dynamics in relation to seasonal variability and upwelling and relaxation patterns at the mouth of Ria de Aveiro (West Iberian margin) over a four-year period. PLoS One, 12: e0177237.

Walker, D. R., and Peterson, W. T. 1991. Relationships between hydrography, phytoplankton production, biomass, cell size and species composition, and copepod production in the southern Benguela upwelling system in April 1988. South African Journal of Marine Science, 11: 289–305.

Widdicombe, C. E., Eloire, D., Harbour, D., Harris, R. P., and Somerfield, P. J. 2010. Long-term phytoplankton community dynamics in the western English Channel. Journal of Plankton Research, 32: 643–655.

Wood, S. N. 2004. Stable and efficient multiple smoothing parameter estimation for generalized additive models. Journal of the American Statistical Association, 99: 673–686.

Xiang, W. 2009. The effect of mesoscale physical processes on microzooplankton group composition and grazing on phytoplankton in summer in the typical waters of South China Sea. Xiamen University Electronic Theses and Dissertations. pp. 18–25.

Xiao, W., Liu, X., Irwin, A. J., Laws, E. A., Wang, L., Chen, B., Zeng, Y. *et al.* 2018a. Warming and eutrophication combine to restructure diatoms and dinoflagellates. Water Research, 128: 206–216.

Xiao, W., Wang, L., Laws, E., Xie, Y., Chen, J., Liu, X., Chen, B. *et al.* 2018b. Realized niches explain spatial gradients in seasonal abundance of phytoplankton groups in the South China Sea. Progress in Oceanography, 162: 223–239.

Yin, K., Qian, P. Y., Wu, M. C. S., Chen, J. C., Huang, L., Song, X., and Jian, W. 2001. Shift from P to N limitation of phytoplankton growth across the Pearl River estuarine plume during summer. Marine Ecology Progress Series, 221: 17–28.

Zeng, X. B., and Huang, B. Q. 2012. Grazing impact of microzooplankton on different pigment groups of phytoplankton in the south Taiwan Strait in summer. Marine Sciences (Chinese), 36: 28–34.

Zeng, X. B., Huang, B. Q., Chen, J. X., and Hong, H. S. 2006. Grazing impact of microzooplankton on algal bloom in the Taiwan Strait in summer. Acta Oceanologica Sinica, 28: 107–116.

Zhang, C., Hong, H., Hu, C., and Shang, S. 2011. Evolution of a coastal upwelling event during summer 2004 in the southern Taiwan Strait. Acta Oceanologica Sinica, 30: 1–6.

Handling editor: Matthew Oliver